Neutron scattering study of the quasi-one-dimensional antiferromagnet $Ba_2CoSi_2O_7$

Minoru Soda,[1,2] Tao Hong,[3] Maxim Avdeev,[4] Hideki Yoshizawa,[1] Takatsugu Masuda,[2] and Hazuki Kawano-Furukawa[1,5]

[1]*RIKEN Center for Emergent Matter Science (CEMS), Wako, Saitama 351-0198, Japan*

[2]*Neutron Science Laboratory, Institute for Solid State Physics, The University of Tokyo, Tokai, Ibaraki 319-1106, Japan*

[3]*Neutron Scattering Science Division, Oak Ridge National Laboratory, Oak Ridge, Tennessee 37831-6393, USA*

[4]*Australian Nuclear Science and Technology Organisation, Locked Bag 2001, Kirrawee DC, New South Wales 2232, Australia*

[5]*Department of Physics, Advanced Sciences, G.S.H.S. Ochanomizu University, Tokyo 112-8610, Japan*

(Received 23 April 2019; revised manuscript received 6 June 2019; published 7 October 2019)

Magnetization and neutron scattering measurements have been carried out on an antiferromagnet $Ba_2CoSi_2O_7$. The observed magnetic excitation is almost dispersionless, and the neutron intensity is only modulated along the [101] direction. The dispersionless magnetic excitation suggest that the $Ba_2CoSi_2O_7$ system is a quasi-one-dimensional antiferromagnet. Classical spin-wave theory for a one-dimensional antiferromagnet can explain the dispersionless spin excitation. The magnetic structure determined by the measurement of the neutron powder diffraction is consistent with no observation of the multiferroic property in this system.

DOI: 10.1103/PhysRevB.100.144410

I. INTRODUCTION

Low-dimensional magnets have been extensively investigated both experimentally and theoretically. For one-dimensional spin systems [1], the Haldane gap and spin-Peierls transition were reported considering the nearest-neighbor interaction while a vector-chiral order, a spin-density wave, and a spin-nematic order were proposed with both nearest-neighbor and next-nearest-neighbor interactions. Two-dimensional spin systems also have interesting magnetic phases with changing magnetic interactions [2]. Therefore, low dimensional magnets are good targets for studying unique magnetic properties.

$Ba_2CoSi_2O_7$ has a two-dimensional network formed by CoO_4 and SiO_4, as shown in Figs. 1(a) and 1(b) [3,4]. $Ba_2CoSi_2O_7$ has a monoclinic structure, and two kinds of Co-Co bonds exist within the b plane. Co^{2+} ion has a spin $S = 3/2$, and a magnetic transition occurs at around 5 K [5]. Similar materials with the Co-square lattice, such as $Ba_2CoGe_2O_7$ and $Ca_2CoSi_2O_7$, show multiferroic properties [6–8], and the local electric polarization of CoO_4 tetrahedra is explained by the spin-dependent d-p hybridization mechanism [9,10]. The magnetic anisotropy also depends on the large single-ion anisotropy D of the easy-plane type and the interaction of local electric polarizations induced by the spin-dependent d-p hybridization mechanism [11,12]. In contrast the anomaly of the dielectric constant in $Ba_2CoSi_2O_7$ was not observed at the transition temperature [5]. The distortion of the crystal structure is expected to affect the magnetic properties significantly, but there is no information about the magnetic structure and interactions in $Ba_2CoSi_2O_7$.

In the present study, the magnetization and neutron scattering measurements were performed to clarify the magnetic model of $Ba_2CoSi_2O_7$. The determined magnetic structure was a collinear antiferromagnetic one with the easy axis along the $[10\bar{1}]$ direction. The observed magnetic excitation is almost dispersionless, but the scattering intensity shows a clear change only along the [101] direction. These results suggest that the $Ba_2CoSi_2O_7$ is the one-dimensional antiferromagnet.

II. EXPERIMENTAL DETAILS

A polycrystalline sample of $Ba_2CoSi_2O_7$ was prepared by solid reaction. $BaCO_3$, CoO, and SiO_2 were mixed with proper molar ratios. The mixtures were sintered at 900 °C for 20 h. The obtained powder was reground and sintered again at 1000 °C for 20 h. The above processes were five times. A single crystal of $Ba_2CoSi_2O_7$ was grown by a floating zone (FZ) method. The initial mixtures were pressed into rod and sintered at 900 °C for 20 h. By using the obtained rod, the single crystal was grown in air.

Magnetization M was measured using a Quantum Design superconducting quantum interference device (SQUID) magnetometer (MPMS) under field-cooling (FC) condition. Neutron powder-diffraction measurement was carried out using the high-resolution powder diffractometer ECHIDNA installed at OPAL, ANSTO, Australia. Neutron with $\lambda = 2.4395$ Å was used. Diffraction patterns were collected at temperatures $T = 1.5$ and 15 K. Neutron scattering measurement on a single crystal was carried out by using a cold-neutron triple-axis spectrometer (CTAX) installed at HFIR, ORNL, USA. The horizontal collimations were set as guide-open-sample-80′-open and a Be filter was placed after the sample. The final neutron energy was fixed at 5.0 meV and the energy resolution at the elastic position was about 0.25 meV. The sample was cooled in a liquid-helium cryostat. The crystals were oriented with the [100] and [001] axes, in one case, and the [101] and [010] axes, in another case, in the scattering plane. It should be noted here that throughout this study, we use the monoclinic unit cell, where lattice parameters are $a = 8.45$ Å, $b = 10.729$ Å, $c = 8.47$ Å, and $\beta = 111.37°$ with space group $C2/c$ [3]. In this used monoclinic unit cell, the $[10\bar{1}]$ direction is almost perpendicular to [101]. Because the lattice constant of the

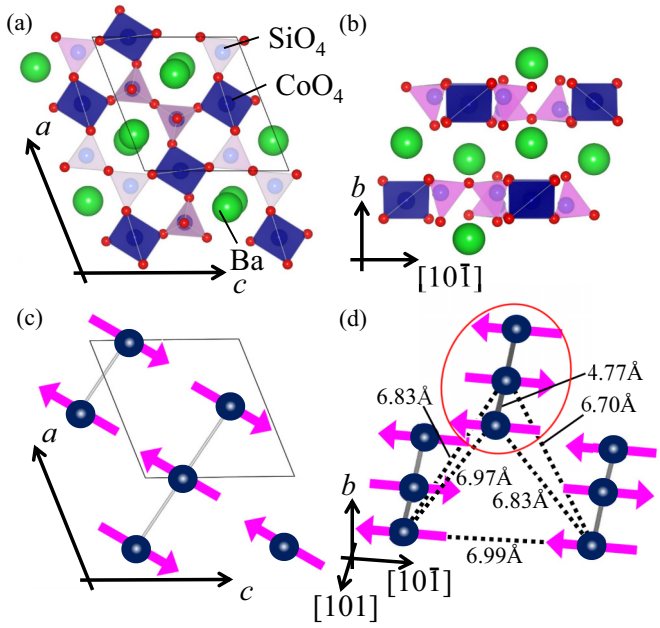

FIG. 1. (a),(b) Crystal structure of $Ba_2CoSi_2O_7$. (c),(d) Schematic magnetic structure of $Ba_2CoSi_2O_7$.

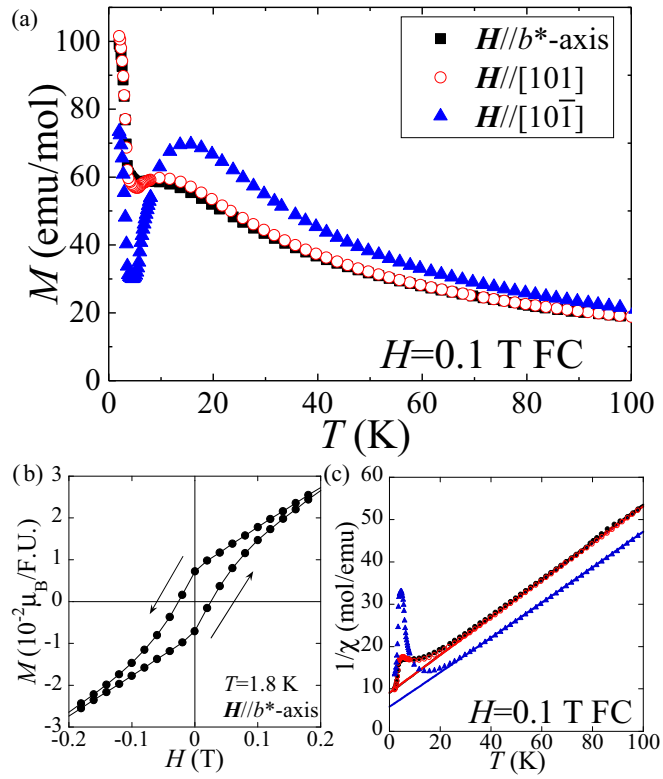

FIG. 2. (a) Temperature dependence of the magnetization taken at $H = 0.1$ T with the magnetic field $H//b^*$, $H//[101]$, and $H//[10\bar{1}]$ under the condition of the field cooling. (b) Magnetic-field dependence of the magnetization at $T = 1.8$ K with the $H//b^*$. (c) Temperature dependence of the inverse magnetic susceptibility. Solid lines show the Curie-Weiss fitting.

a axis is almost equal to that of the c axis, it is difficult to distinguish between the a and c axes in the present study.

III. RESULTS

A. Magnetization

Figure 2(a) shows the temperature dependence of the magnetization taken at $H = 0.1$ T under FC condition. The magnetization with $H//[10\bar{1}]$ shows a broad peak at approximately $T = 15$ K, which is different from the magnetizations with $H//b^*$ and $H//[101]$. This means that the $Ba_2CoSi_2O_7$ has large magnetic anisotropy. Below 5 K, a weak ferromagnetic component was observed in all directions. Figure 2(b) shows the magnetic field dependence of the magnetization with $H//b^*$ at $T = 1.8$ K. The magnitude of the ferromagnetic component is approximately $0.01\mu_B$/Co. Because there is no anisotropy associated with small levels of ferromagnetism below 5 K, the ferromagnetic component may be induced by a small impurity. In contrast, the magnetization data reported by Akaki *et al.* shows no magnetic anisotropy nor any ferromagnetic component [5]. The cause of this difference in magnetic anisotropy is not clear.

The temperature dependence of the inverse magnetic susceptibility, $(M/H)^{-1}$, is plotted in Fig. 2(c), and the data above 50 K were fitted by Curie-Weiss law including the χ_0 constant. The g values estimated from the Curie constant are 2.18, 2.20, and 2.31 for $H//b^*$ axis, $H//[101]$, and $H//[10\bar{1}]$, respectively. The large g values are almost consistent with the previous polycrystalline study [3]. The $[10\bar{1}]$ axis is expected to be a characteristic one in $Ba_2CoSi_2O_7$. The anisotropy of the g value in $Ba_2CoSi_2O_7$ is totally different from that in $Ba_2CoGe_2O_7$ [13].

B. Powder neutron diffraction

Figure 3(a) shows the neutron powder-diffraction pattern measured at 15 K. The inset shows the calculated intensity on the basis of crystal structure with the space group $C2/c$ [3]. The observed neutron-diffraction pattern is reproduced roughly by the reported crystal structure. However, reflections indicated by solid arrows cannot be explained by $Ba_2CoSi_2O_7$ with the reported crystal structure nor by materials with the similar chemical formulas, $BaCoSi_2O_7$ [3] and $BaCoSiO_4$ [14]. Because the main purpose of the present study is a clarification of the magnetic property rather than a detailed crystal structure analysis, we consider only the neutron intensities that demonstrate a temperature dependence. The unspecified phase indicated by solid arrows may have a ferromagnetic component observed in the magnetization, however, the quite small ferromagnetic component cannot be confirmed in the present neutron study. In the magnetic structure analysis, the reported atomic positions were applied to Co ions [3], and the nuclear intensities were used only as a scaling factor to estimate the magnitude of the magnetic moment.

Figure 3(b) shows the neutron powder-diffraction pattern measured at 1.5 K. As indicated by dashed arrows, several magnetic reflections were observed in the low-angle region. Figure 3(c) shows the magnetic intensities obtained by subtracting the data at 15 K from those at 1.5 K. All magnetic peaks are indexed by the propagation vector (1/2, 1/2, 1/2).

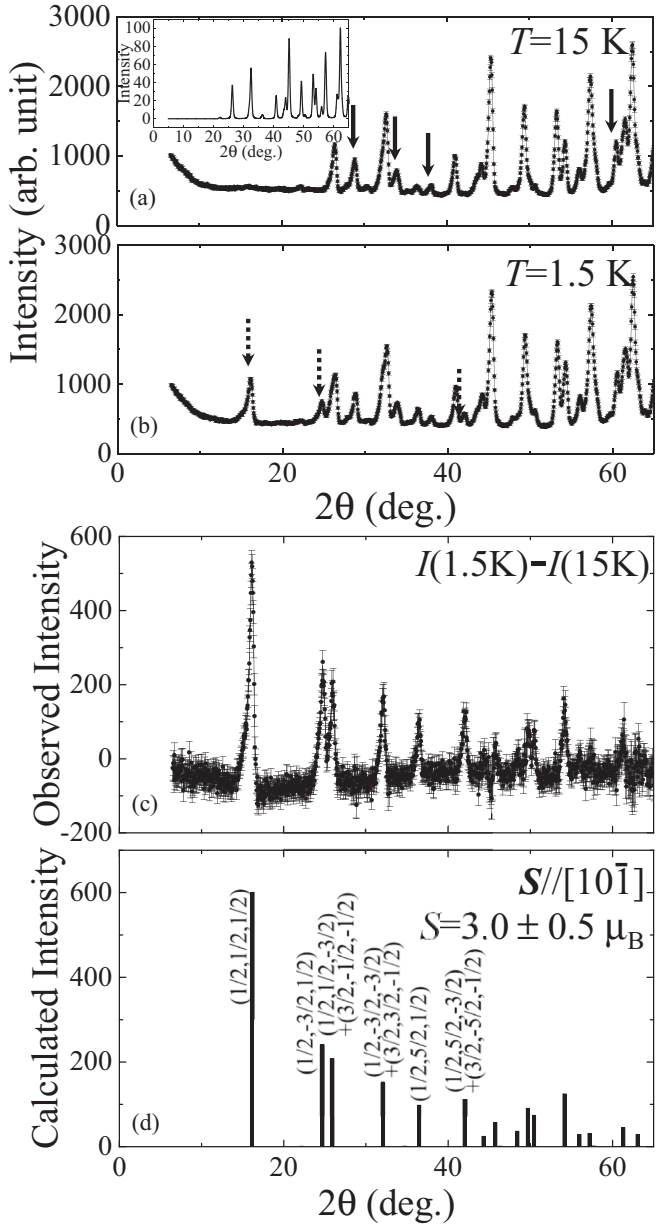

FIG. 3. (a) Neutron powder-diffraction patterns measured at 15 K. Solid arrows indicate the unidentified peaks. Inset shows the calculated intensity with the reported structure. (b) Neutron powder-diffraction patterns measured at 1.5 K. Dashed arrows indicate the magnetic reflections. (c) Magnetic intensities obtained by subtracting the data at 15 K from those at 1.5 K. (d) Magnetic intensities calculated for the collinear antiferromagnetic structure with the easy axis along the [10$\bar{1}$].

C. Neutron scattering on single crystal

The temperature dependence of the magnetic Bragg intensity at $(1/2, 1/2, 1/2)$ measured using a single crystal is shown in Fig. 4(a). With decreasing T, the large-intensity component due to magnetic ordering appears below $T_N =$ 6 K. Note that magnetic reflections were observed at both $(1/2, 1/2, 1/2)$ and $(1/2, -1/2, 1/2)$, which provides information about crystal domains.

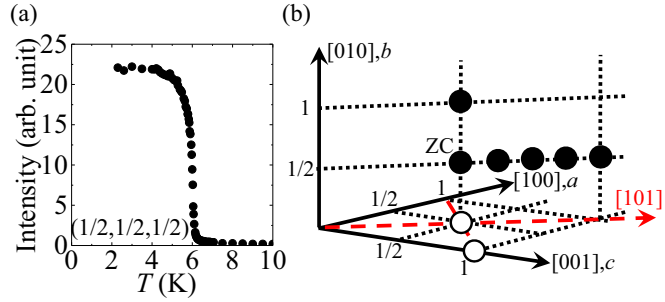

FIG. 4. (a) Temperature dependence of the magnetic Bragg intensity at $(1/2, 1/2, 1/2)$. (b) $\boldsymbol{Q}$ points of profiles measured in Figs. 5 and 6(a). Closed and opened circles show $\boldsymbol{Q}$ points measured in scans with $(h\ k\ h)$ and $(h\ 0\ l)$ scattering planes, respectively.

Figure 5(a) shows the constant-$\boldsymbol{Q}$ scan profiles at $(1/2, 1/2, 1/2)$ measured at 1.5 ($<T_N$) and 15 K ($>T_N$). At 1.5 K, a small peak at $\hbar\omega = 1$ meV, a sharp peak at $\hbar\omega =$ 2.9 meV, and a broad peak at $\hbar\omega = 4$ meV were observed. The peak at $\hbar\omega = 2.9$ meV disappears at 15 K. Therefore, we attribute only the excitation at $\hbar\omega = 2.9$ meV to the magnetic origin.

The $\boldsymbol{Q}$ dependencies of the magnetic excitations along the b^*, [10$\bar{1}$], and [101] directions were measured at 1.5 K to examine the dispersion of the magnetic excitation. The closed and opened circles in Fig. 4(b) show the measured $\boldsymbol{Q}$ points in the $(h\ k\ h)$ and $(h\ 0\ l)$ scattering planes, respectively. The neutron profiles shown in Figs. 5(a) and 5(b) were measured in the $(h\ k\ h)$ scattering plane, and the $\boldsymbol{Q}$ point (1/2,1,1/2) shown in Fig. 5(b) corresponds to zone-boundary position with $\boldsymbol{q} = (0, 1/2, 0)$ from the magnetic zone center $(1/2, 1/2, 1/2)$. The $\boldsymbol{Q}$ points shown in Figs. 5(c) and 5(d), which were measured in the $(h\ 0\ l)$ scattering plane, were $(1/2, 0, 1/2)$ and (0,0,1), respectively, and the $\boldsymbol{Q}$ point (0,0,1) corresponds to $(1/2, 0, 1/2)$–$(1/2, 0, -1/2)$. These results reveal that both the neutron intensity and peak energy show less change along the b^* and [10$\bar{1}$] directions. We note that only the peak at $\hbar\omega = 2.9$ meV shows a temperature dependence even at $(1/2, 0, 1/2)$, as shown in Fig. 5(c). Figure 6(a) shows the constant-$\boldsymbol{Q}$ scan profiles measured at $(h, 1/2, h)$, which correspond to the $\boldsymbol{Q}$ dependence along the [101] direction. Figure 6(b) shows the h dependence of integrated intensities and peak energies obtained by Gaussian fitting of the constant-$\boldsymbol{Q}$ profiles at $(h, 1/2, h)$. The excitation observed at $\hbar\omega =$ 2.9 meV is almost dispersionless, which is similar to the excitation of the local mode. On the other hand, the integrated intensity exhibits a clear modulation along the [101] direction.

The $\boldsymbol{Q}$ dependences of the intensities with $\hbar\omega = 2.9$ meV along the [101] direction at (h, k, h) with $k = 1/2$, 1, and 3/2 are shown in Fig. 6(c). The background (BG) intensity, about 10–15 in Fig. 6(c), was taken from the constant-$\boldsymbol{Q}$ scans shown in Fig. 6(a). The magnetic excitation exhibits the large intensity near $(1/2, k, 1/2)$ and $(3/2, k, 3/2)$, with a minimum intensity near $(1, k, 1)$. This result suggests that the magnetic excitation shows a modulation in which $\boldsymbol{q}$ corresponds to the nearest-neighbor Co ions along the [101] direction.

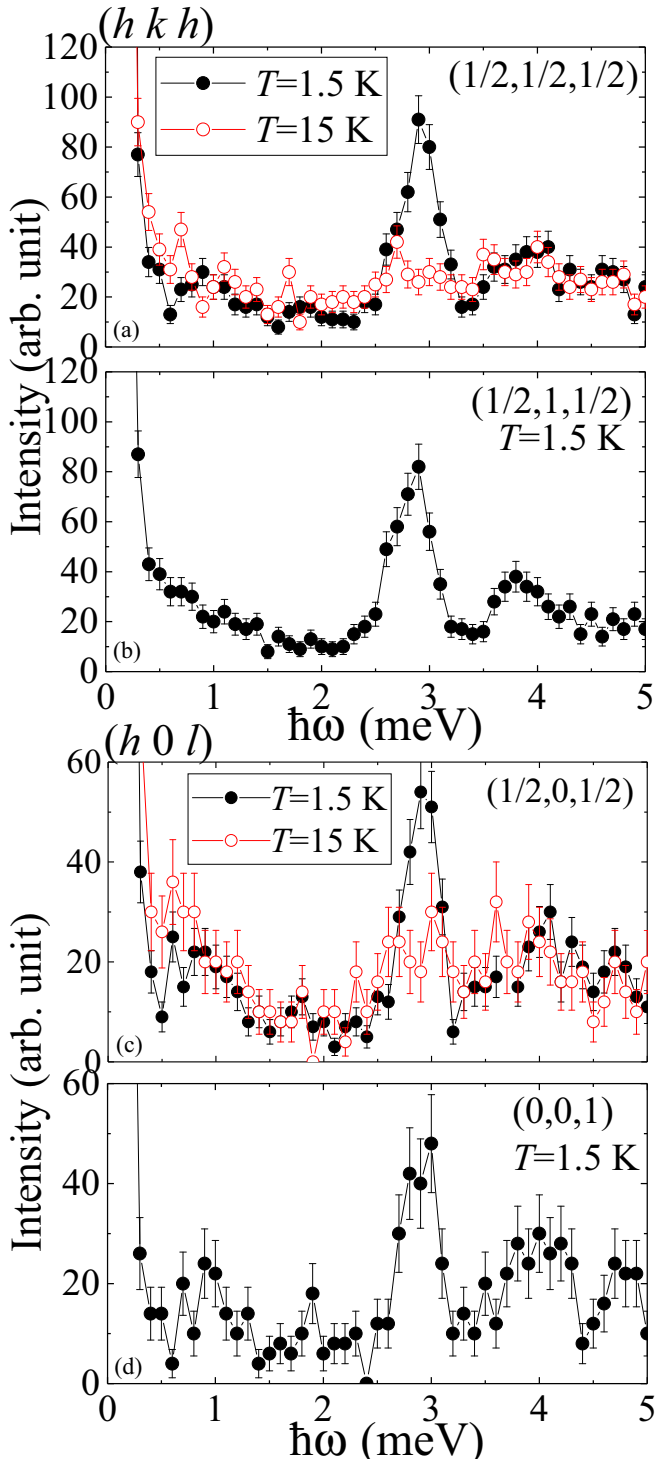

FIG. 5. (a),(b) Constant-$\boldsymbol{Q}$ scans at (a) (1/2, 1/2, 1/2) and (b) (1/2, 1, 1/2) measured in (h k h) plane. (c),(d) Constant-$\boldsymbol{Q}$ scans at (c) (1/2, 0, 1/2) and (d) (0,0,1) measured in (h 0 l) plane.

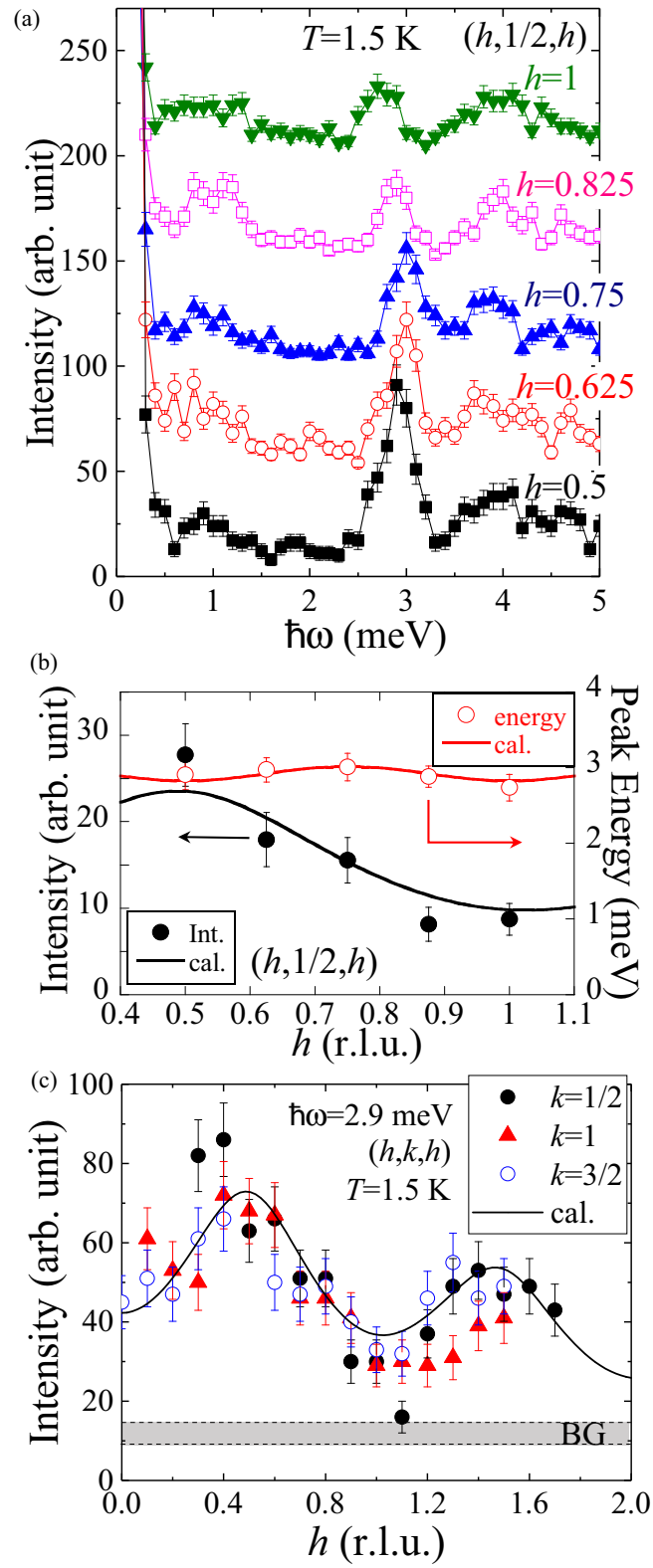

FIG. 6. (a) Constant-$\boldsymbol{Q}$ scans at (h, 1/2, h) measured at 1.5 K. Data are shifted by vertical offsets. (b) Integrated intensities and the peak energies obtained by the Gaussian fitting of constant-$\boldsymbol{Q}$ scans at (h, 1/2, h). Solid lines are the calculated values with the classical spin-wave theory. (c) Neutron intensities at (h, k, h) with keeping $\hbar\omega = 2.9$ meV against h for $k = 1/2$, 1, and 3/2. Solid line shows the calculation with the classical spin-wave theory for $k = 1/2$.

IV. ANALYSIS AND DISCUSSION

We determine the magnetic structure of $Ba_2CoSi_2O_7$ by considering the magnetic reflections observed in the powder neutron-diffraction experiment. To explain the magnetic reflections shown in Fig. 3(c), we applied the magnetic structure shown in Figs. 1(c) and 1(d). Figure 3(d) presents the

calculated magnetic intensities and the indices of the magnetic reflections in the low-angle region. The observed magnetic intensities are reproduced perfectly by the collinear antiferromagnetic structure with the easy axis along the $[10\bar{1}]$. In the calculation, the isotropic magnetic form factor of Co^{2+} was used [15]. The estimated magnitude of the Co magnetic moment is $3.0(5)\mu_B$.

The magnetic structure shown in Fig. 1(d) induces the magnetic reflection at $(1/2, 1/2, 1/2)$ while the magnetic structure with oppositely oriented spins in the red circle induces the magnetic reflection at $(1/2, -1/2, 1/2)$. One of the two magnetic structures should be stabilized because the distances between the Co ions are not uniform, as shown in Fig. 1(d). However, the $|\boldsymbol{Q}|$ values for the $(1/2, 1/2, 1/2)$ and $(1/2, -1/2, 1/2)$ reflections are the same, and the two magnetic structures exhibit quite similar neutron intensities. In the single-crystal experiment, furthermore, we observed the magnetic reflections at both $(1/2, 1/2, 1/2)$ and $(1/2, -1/2, 1/2)$, which can be attributed to twin crystals. Then, we could not determine the exact arrangements of the magnetic moments along the b axis.

In the neutron powder-diffraction experiment, we found that $Ba_2CoSi_2O_7$ has a collinear antiferromagnetic structure with the easy axis along the $[10\bar{1}]$, and that the spins demonstrate an antiferromagnetic arrangement along [101] and a ferromagnetic arrangement along $[10\bar{1}]$. In the spin-dependent d-p hybridization mechanism [9,10], the local electric polarization of the CoO_4 tetrahedron is almost zero with the magnetic moment along $[10\bar{1}]$. Furthermore, even if the magnetic moment rotates within the b plane under the magnetic field the antiferroelectric state would be realized. The dielectric property in $Ba_2CoSi_2O_7$ is much different from that in $Ba_2CoGe_2O_7$ [6,11,12].

Next we discuss the magnetic model including the magnetic interaction in $Ba_2CoSi_2O_7$, by using the following spin Hamiltonian:

$$\mathcal{H} = J\sum_i \left[S_i^z S_{i+1}^z + \epsilon\left(S_i^x S_{i+1}^x + S_i^y S_{i+1}^y\right)\right] + \sum_i D\left(S_i^z\right)^2. \quad (1)$$

The spins are aligned with the z axis. J is the exchange interaction and D is the single ion anisotropy. In the classical spin-wave theory the spin Hamiltonian with the Holstein-Primakoff transformation is written as

$$\mathcal{H} = \sum_{\boldsymbol{q}} \left(A_{\boldsymbol{q}} a_{\boldsymbol{q}}^\dagger a_{\boldsymbol{q}} + \tfrac{1}{2} B_{\boldsymbol{q}} (a_{\boldsymbol{q}} a_{-\boldsymbol{q}} + a_{\boldsymbol{q}}^\dagger a_{-\boldsymbol{q}}^\dagger)\right), \quad (2)$$

where

$$A_{\boldsymbol{q}} = 2S[J(0) - D], \quad (3)$$

$$B_{\boldsymbol{q}} = 2S\epsilon J(\boldsymbol{q}). \quad (4)$$

The energy of the magnetic excitation is

$$(\hbar\omega_{\boldsymbol{q}})^2 = A_{\boldsymbol{q}}^2 - B_{\boldsymbol{q}}^2. \quad (5)$$

One magnon cross section is

$$\left(\frac{d^2\sigma}{d\Omega dE'}\right) \propto \left(C_1 \frac{A_{\boldsymbol{q}} + B_{\boldsymbol{q}}}{\sqrt{A_{\boldsymbol{q}}^2 - B_{\boldsymbol{q}}^2}} + C_2 \frac{A_{\boldsymbol{q}} - B_{\boldsymbol{q}}}{\sqrt{A_{\boldsymbol{q}}^2 - B_{\boldsymbol{q}}^2}}\right)\delta(\hbar\omega - \hbar\omega_{\boldsymbol{q}}), \quad (6)$$

where C_1 and C_2 are constant. To explain the dispersionless magnetic excitation we consider the one-dimensional antiferromagnet in which the antiferromagnetic chain is along the [101] direction. In Eq. (1), the Ising-like antiferromagnet with $\epsilon < 1$ and $D = 0$ leads to the exact same result as that for the easy-axis antiferromagnet with $\epsilon = 1$ and $D < 0$. We cannot distinguish two models in the classical spin-wave theory. It should be noted that the observed magnetic excitation cannot be explained by the easy-plane anisotropy model used in $Ba_2CoGe_2O_7$ [11]. We performed the calculations of the neutron intensity and the dispersion energy for both the easy-axis and Ising-like antiferromagnet models. In the calculation, the isotropic magnetic form factor of Co^{2+} was used [15]. The magnetic dispersion relation shown in Fig. 6(b) is reproduced by the one-dimensional antiferromagnet model, as shown by solid curves. In the easy-axis antiferromagnet model, the parameters were $J = 0.35 \pm 0.09$ meV and $D = -0.65 \pm 0.07$ meV while in the Ising-like antiferromagnet model, $J = 1.00 \pm 0.02$ meV and $\epsilon = 0.35 \pm 0.08$. By using the same parameters, the neutron intensity along $(h, 1/2, h)$ was also calculated in Fig. 6(c). These analyses indicate that the one-dimensional antiferromagnet with the easy-axis spin anisotropy or the Ising-like spin is realized in $Ba_2CoSi_2O_7$ although the modulation of the observed neutron intensities is slightly larger than that of the calculated intensity. On the other hand, the long-ranged magnetic order below T_N indicates an existence of the magnetic interaction between the one-dimensional chains. However, both the neutron intensity and excitation energy show less change along the interchain, indicating that the interaction between the chains is very small. Then, we could not estimate the interaction between the chains.

Here we consider the possibilities of the easy-axis and Ising-like antiferromagnet models. The CoO_4 tetrahedra in $Ba_2CoSi_2O_7$ is distorted [3], and the g values estimated from the Curie constant are anisotropic. These indicate that the component of the single-ion anisotropy is not zero. Furthermore, the magnetic dispersion in $Ba_2CoSi_2O_7$ is not consistent with the model of the motion of domain-wall pairs, which has been reported in one-dimensional Ising-type antiferromagnet $CsCoCl_3$ [16–19]. Although we cannot distinguish the easy-axis and Ising-like antiferromagnet models in the present neutron study, the one-dimensional antiferromagnet model with the easy-axis anisotropy is expected to be better.

Our results of the neutron scattering suggest that the $Ba_2CoSi_2O_7$ is the one-dimensional antiferromagnet with the easy-axis spin anisotropy or the Ising-like spin. On the other hand, tetragonal or orthorhombic åkermanite-type materials, such as $Ba_2CoGe_2O_7$ [11,12,20] and $Ca_2CoSi_2O_7$ [8,21], serve as two-dimensional easy-plane antiferromagnets. The åkermanite-type materials have two kinds of Co-Co networks, CoO_4-SiO_4-CoO_4 (or CoO_4-GeO_4-CoO_4) and CoO_4-SiO_4-SiO_4-CoO_4 (or CoO_4-GeO_4-GeO_4-CoO_4). The neutron results suggest that the network of CoO_4-SiO_4-CoO_4 serve as the main magnetic interaction, highlighting the difference between one- and two-dimensional antiferromagnets. Furthermore, the magnetic anisotropy is expected to depend on the distortion of CoO_4. In åkermanite-type materials, the crystal structure affects both the magnetic interaction dimensionality and anisotropy.

V. CONCLUSION

Neutron scattering study has been carried out on the powder and the single-crystal $Ba_2CoSi_2O_7$ samples. The results revealed that the collinear antiferromagnetic structure with the easy axis along the $[10\bar{1}]$ direction is realized below 6 K. The observed magnetic excitation is dispersionless, but the neutron intensity of the magnetic excitation has a $|\boldsymbol{Q}|$ dependence along the [101] direction. Our neutron results show that the $Ba_2CoSi_2O_7$ is the one-dimensional antiferromagnet.

ACKNOWLEDGMENTS

The neutron experiment on CTAX was supported by the US-Japan Cooperative Program on Neutron Scattering. The alignment of the single crystal was carried out using the CG-1B installed at ORNL. A portion of this research used resources at the High Flux Isotope Reactor, a DOE Office of Science User Facility operated by the Oak Ridge National Laboratory. This work was supported by KAKENHI (Grant No. 15K05123).

[1] H.-J. Mikeska and A. K. Kolezhuk, Lect. Notes Phys. **645**, 1 (2004).
[2] J. Richter, J. Schulenburg, and A. Honecker, Lect. Notes Phys. **645**, 85 (2004).
[3] R. D. Adams, R. Layland, C. Payen, and T. Datta, Inorg. Chem. **35**, 3492 (1996).
[4] K. Momma and F. Izumi, J. Appl. Crystallogr. **44**, 1272 (2011).
[5] M. Akaki, J. Tozawa, D. Akahoshi, and H. Kuwahara, J. Phys.: Conf. Ser. **150**, 042001 (2009).
[6] H. Murakawa, Y. Onose, S. Miyahara, N. Furukawa, and Y. Tokura, Phys. Rev. Lett. **105**, 137202 (2010).
[7] H. T. Yi, Y. J. Choi, S. Lee, and S.-W. Cheong, Appl. Phys. Lett. **92**, 212904 (2008).
[8] M. Akaki, H. Kuwahara, A. Matsuo, K. Kindo, and M. Tokunaga, J. Phys. Soc. Jpn. **83**, 093704 (2014).
[9] C. Jia, S. Onoda, N. Nagaosa, and J. H. Han, Phys. Rev. B **76**, 144424 (2007).
[10] T. Arima, J. Phys. Soc. Jpn. **76**, 073702 (2007).
[11] M. Soda, M. Matsumoto, M. Månsson, S. Ohira-Kawamura, K. Nakajima, R. Shiina, and T. Masuda, Phys. Rev. Lett. **112**, 127205 (2014).
[12] M. Soda, S. Hayashida, B. Roessli, M. Månsson, J. S. White, M. Matsumoto, R. Shiina, and T. Masuda, Phys. Rev. B **94**, 094418 (2016).
[13] V. Hutanu, A. P. Sazonov, M. Meven, G. Roth, A. Gukasov, H. Murakawa, Y. Tokura, D. Szaller, S. Bordács, I. Kézsmárki, V. K. Guduru, L. C. J. M. Peters, U. Zeitler, J. Romhányi, and B. Náfrádi, Phys. Rev. B **89**, 064403 (2014).
[14] B. Liu and J. Barbier, J. Solid State Chem. **102**, 115 (1993).
[15] P. J. Brown, *International Tables for Crystallography*, edited by A. J. C. Wilson (Kluwer, Dordrecht, 1992), Vol. C, Chap. 4.
[16] N. Ishimura and H. Shiba, Prog. Theor. Phys. **63**, 743 (1980).
[17] H. Shiba, Prog. Theor. Phys. **64**, 466 (1980).
[18] S. K. Satija, G. Shirane, H. Yoshizawa, and K. Hirakawa, Phys. Rev. Lett. **44**, 1548 (1980).
[19] H. Yoshizawa, K. Hirakawa, S. K. Satija, and G. Shirane, Phys. Rev. B **23**, 2298 (1981).
[20] M. Soda, L. J. Chang, M. Matsumoto, V. O. Garlea, B. Roessli, J. S. White, H. Kawano-Furukawa, and T. Masuda, Phys. Rev. B **97**, 214437 (2018).
[21] M. Soda, S. Hayashida, T. Yoshida, M. Akaki, M. Hagiwara, M. Avdeev, O. Zaharko, and T. Masuda, J. Phys. Soc. Jpn. **86**, 064703 (2017).